Journal of Alloys and Compounds 652 (2015) 91–99

Contents lists available at ScienceDirect

Journal of Alloys and Compounds

journal homepage: http://www.elsevier.com/locate/jalcom

# Solvothermal synthesis of zinc oxide microspheres

Ankica Šarić [a, *], Goran Štefanić [a], Goran Dražić [b], Marijan Gotić [a]

[a] Division of Materials Chemistry, Ruđer Bošković Institute, Bijenička 54, P.O. Box 180, HR-10002 Zagreb, Croatia
[b] National Institute of Chemistry, Hajdrihova 19, SI-1001 Ljubljana, Slovenia

ARTICLE INFO

*Article history:*
Received 2 June 2015
Accepted 24 August 2015
Available online 28 August 2015

*Keywords:*
Nanostructured materials
Oxide materials
Microstructure
Optical properties
Scanning electron microscopy
SEM
X-ray diffraction

ABSTRACT

The solvothermal synthesis of ZnO particles from zinc acetylacetonate [$Zn(acac)_2$] in the presence of triethanolamine (TEA) and various solvent systems at 170 °C is reported. The structural, optical and morphological characteristics of ZnO particles were investigated. It was found that the size and shape of ZnO nanoparticles and the way of their aggregation depend on the mole ratio [TEA]/[$Zn(acac)_2$] and the type of alcohol used as a solvent. Doubling the molar ratio of TEA to $Zn(acac)_2$ in the presence of ethanol favoured the formation of huge spherical aggregates (>3 μm) assembled from fine and uniform ZnO nanoparticles (~20 nm). The results of present investigation show a strong impact of surface interactions between the formed ZnO nanoparticles and the molecules of solvent and TEA on the way of growth and aggregation, which enables the control of their morphological properties. The results show that TEA serves as a link between primary ZnO nanoparticles to form spherical aggregates with a controllable diameter. The results of X-ray diffraction size-strain analysis indicate the presence of size anisotropy with bigger crystallites in the direction of the c-ax of the zincite lattice compared with the direction perpendicular to the c-ax. The red shift of the absorption edge and reduced band gap energies are clearly visible with the increased sample microsphere size.



## 1. Introduction

Zinc oxide (ZnO) is an important material with powerful optical, electrical, and structural properties. Morphologically it is a very attractive compound that possesses thermal and chemical stability. Due to these unique characteristics zinc oxide is a commercially exploited material with a wide range of applications such as LEDs, gas or UV sensors, catalysts, varistors, photodetectors, paints, cosmetics, rubber, solar cells, detectors, etc. Moreover, due to its nontoxicity and high photocatalytic activity, ZnO is increasingly used for the degradation of various environmental pollutants [1,2].

To develop size and morphology controlled ZnO nanoparticles, synthesis route is of major importance [3]. For instance, Verges et al. [4] synthesized rod-like zinc-oxide nanoparticles obtained from the hydrolysis of zinc nitrate and zinc chloride in the presence of hexamethylenetetramine. Wu and Wu [5] used the hydrothermal method with a $ZnCl_2 \cdot Zn(OH)_2$ compound as the precursor for the synthesis of ZnO nanorods. Yu and Yu [6] hydrothermally synthesized ZnO hollow spheres with porous crystalline shell starting from the $ZnCl_2$/glucose precursor. The synthesized ZnO spheres were used for the decolourization of the Rhodamine B aqueous solution. The results showed that hollow spheres could be more readily separated from the slurry system by filtration or sedimentation after a photocatalytic reaction and reused than a conventional powder photocatalyst. Cho et al. [7] reported about the high influence of citric acid and various citrates on the nucleation, growth and shape of ZnO crystals. The hydrolysis of zinc acetylacetonate monohydrate in the presence of citrate anions yielded square plate-like ZnO particles [8]. Nanosize ZnO particles were prepared by the thermal decomposition of zinc acetylacetonate monohydrate [9], whereas its simple hydrolysis in aqueous media at 90 °C yielded hollow tubular ZnO particles [10].

Among the various organic additives used to date, a versatile family of ethanolamines that combine the properties of amines and alcohols have found important applications, since they induce a considerable change in particle surface properties [11–14]. Diethanolamine (DEA) [13] or triethanolamine (TEA) [11,12] were used as polymerization agents and stabilizers to control the morphology of the ZnO microsphere assembled by the aggregation of primary nanoparticles. Triethanolamine as a complexing agent enhances the doping probability of the formed Sb-doped ZnO nanopowder [14]. Fu et al. [15] proposed a growth mechanism of spherical

* Corresponding author.
*E-mail address:* asaric@irb.hr (A. Šarić).

http://dx.doi.org/10.1016/j.jallcom.2015.08.200
0925-8388/

agglomerates with 200 nm in diameter, generated by the oriented attachment of 4–6 nm ZnO nanoparticles in a mixed water-isopropanol system using triethanolamine. It was suggested that the selective adsorption of triethanolamine molecules on crystallographic planes plays an important role in their oriented attachment, leading to the formation of flocky spheres with a single-crystal structure. On the other hand, Yao et al. [16] reported about the synthesis of biphasic nanocomposites of ZnO-poly(vinilpyrrolidone) which exhibited twinned pseudospherical morphology in the range of 100 nm to several micrometres. The combination of oriented attachment together with the Ostwald ripening of small primary particles in a later stage of the reaction produced a cavity inside the spherical mesocrystals.

In this research we investigated the impact of several important processing parameters (the presence of TEA as a grown particle modifier, the presence of $acac^-$ ligands and the presence of solvent molecules of different size and polarity) on the structural and microstructural properties of the obtained ZnO particles. The aim of the investigation was to achieve a good control of the size and morphology of primary ZnO nanoparticles and the way of their aggregation.

## 2. Experimental

### 2.1. Preparation of samples

Zinc acetylacetonate monohydrate ($Zn(C_5H_7O_2)_2 \cdot H_2O$; *Alfa Aeser®*), triethanolamine ($C_6H_{15}NO_3$; *Kemika*) absolute ethanol ($C_2H_5OH$; *Kemika*) and 1-octanol ($CH_3(CH_2)_7OH$; *Sigma Aldrich*), all of analytical purity were used.

The experiments were divided into three groups. Sample notation and the conditions used for their preparation are given in Table 1. The first series of samples was synthesized by adding $Zn(acac)_2$ (0.5 g) to ethanol (30 ml) and autoclaving at 170 °C for 4, 24 or 72 h (samples E1, E2 and E3, respectively). The second series of samples was synthesized by adding $Zn(acac)_2$ (0.5 g) to octanol (30 ml) and autoclaving at 170 °C for 4, 24 or 72 h (samples O1, O2 and O3, respectively). The third series of samples was synthesized in the presence of triethanolamine (TEA). Firstly, the triethanolamine (TEA) was dissolved in ethanol. Then $Zn(acac)_2 \cdot H_2O$ was added to this solution and the molar ratio of TEA to $Zn(acac)_2 \cdot H_2O$ was adjusted to 1:2, 1:1 and 2:1 (TEA/ethanol precursor solutions). Thus prepared transparent precursor solution was autoclaved at 170 °C for 4, 24 or 72 h (samples ET). In the same way the TEA/octanol precursor solutions were prepared and autoclaved at 170 °C for 4, 24 or 72 h (samples OT). A 50 mL Teflon-lined stainless steel autoclave was used. After autoclaving, the obtained precipitates were centrifuged and washed several times with ethanol, then dried.

**Table 1**
The notation and experimental conditions used for the preparation of ZnO samples. Each precipitation system contained 0.5 g of $Zn(acac)_2$. Ageing temperature was 170 °C.

| Sample | [TEA]/[$Zn(acac)_2$] | Ethanol/ml | Octanol/ml | $t_{ageing}$/h |
|---|---|---|---|---|
| E1 | 0 | 30 | | 4 |
| E2 | 0 | 30 | | 24 |
| E3 | 0 | 30 | | 72 |
| O1 | 0 | | 30 | 4 |
| O2 | 0 | | 30 | 24 |
| O3 | 0 | | 30 | 72 |
| ET1 | 1:2 | 30 | | 4 |
| ET2 | 1:2 | 30 | | 24 |
| ET3 | 1:2 | 30 | | 72 |
| ET4 | 1:1 | 30 | | 4 |
| ET5 | 1:1 | 30 | | 24 |
| ET6 | 1:1 | 30 | | 72 |
| ET7[a] | 2:1 | 30 | | 4 |
| ET8 | 2:1 | 30 | | 24 |
| ET9 | 2:1 | 30 | | 72 |
| OT1 | 1:2 | | 30 | 4 |
| OT2 | 1:2 | | 30 | 24 |
| OT3 | 1:2 | | 30 | 72 |
| OT4[a] | 1:1 | | 30 | 4 |
| OT5 | 1:1 | | 30 | 24 |
| OT6 | 1:1 | | 30 | 72 |
| OT7[a] | 2:1 | | 30 | 4 |
| OT8[a] | 2:1 | | 30 | 24 |
| OT9[a] | 2:1 | | 30 | 72 |

[a] There was no precipitation.

### 2.2. Characterization of samples

XRD patterns were recorded using *Italstructures* X-ray powder diffractometer (APD 2000, Cu-$K_\alpha$ radiation, graphite monochromator, scintillation detector). FT-IR spectra were recorded using a *Perkin Elmer* spectrometer (model 2000). UV/Vis spectra were recorded by a *Shimadzu* UV/Vis/NIR spectrometer equipped with an integrated sphere (model UV-3600). The microstructural characterization of samples was performed using a Field Emission Scanning Electron Microscope (FE-SEM) model JSM-7000F and a probe Cs corrected Scanning Transmission Electron Microscope, model ARM 200 CF, manufactured by *Jeol Ltd*.

## 3. Results

### 3.1. Electron microscopy analysis

Fig. 1 shows the SEM images of ZnO particles in samples E3, ET3 and ET6. Sample E3, prepared in ethanol without TEA, (Fig. 1a) mostly consists of rod-like nanoparticles about 100 nm long with the aspect ratio (length/width) around 2–3. There is a high tendency of lateral aggregation. With the addition of a small amount of TEA the size (~20 nm) of rod-like nanoparticles decreased significantly (sample ET3, Fig. 1b). Fig. 1c and d shows the SEM images of sample ET6 prepared at the mole ratio [TEA]/[$Zn(acac)_2$] = 1:1. At lower magnification (Fig. 1c) the large regular spheres of ~1 μm in size dominate, but the cracked spheres and much smaller irregular nanoparticle aggregates are also visible. At higher magnification discrete particles on the surface of one sphere become well-visible (Fig. 1d).

Fig. 2 shows the SEM images of ZnO particles in sample ET8 prepared at the mole ratio [TEA]/[$Zn(acac)_2$] = 2:1. Fig. 2a shows the characteristic big sphere ~3.5 μm in size with a clearly visible fissure. Small irregular aggregates on the surface of the crack are also visible. Fig. 2b shows a half of the cracked sphere. One can see that the interior of the sphere consists of the same small nanosized particles that can be found on the surface. The configuration of the fracture is characterised by a number of slots (channels) that are oriented from the centre of the sphere to its surface. Fig. 2c is a magnified image showing the size and morphology of discrete and uniform nanosized ZnO particles that constitute big spheres of sample ET8.

Fig. 3 shows the SEM images of ZnO particles in samples O3, OT3 and OT6 prepared in octanol. Sample O3, prepared without TEA, consists of (i) discrete rod-like nanoparticles ~100 nm in size forming very weak bounded irregular aggregates, and (ii) bigger spherical aggregates ~0.5 μm in size, shaped from the same rod-like nanoparticles (Fig. 3a). Sample OT3, prepared in the presence of a small amount of TEA (mole ratio [TEA]/[$Zn(acac)_2$] = 1:2), consists of small irregular spheres about 100 nm in size made up of loosely aggregated rod-like nanoparticles (Fig. 3b). Sample OT6, synthesized in the presence of TEA at the mole ratio [TEA]/

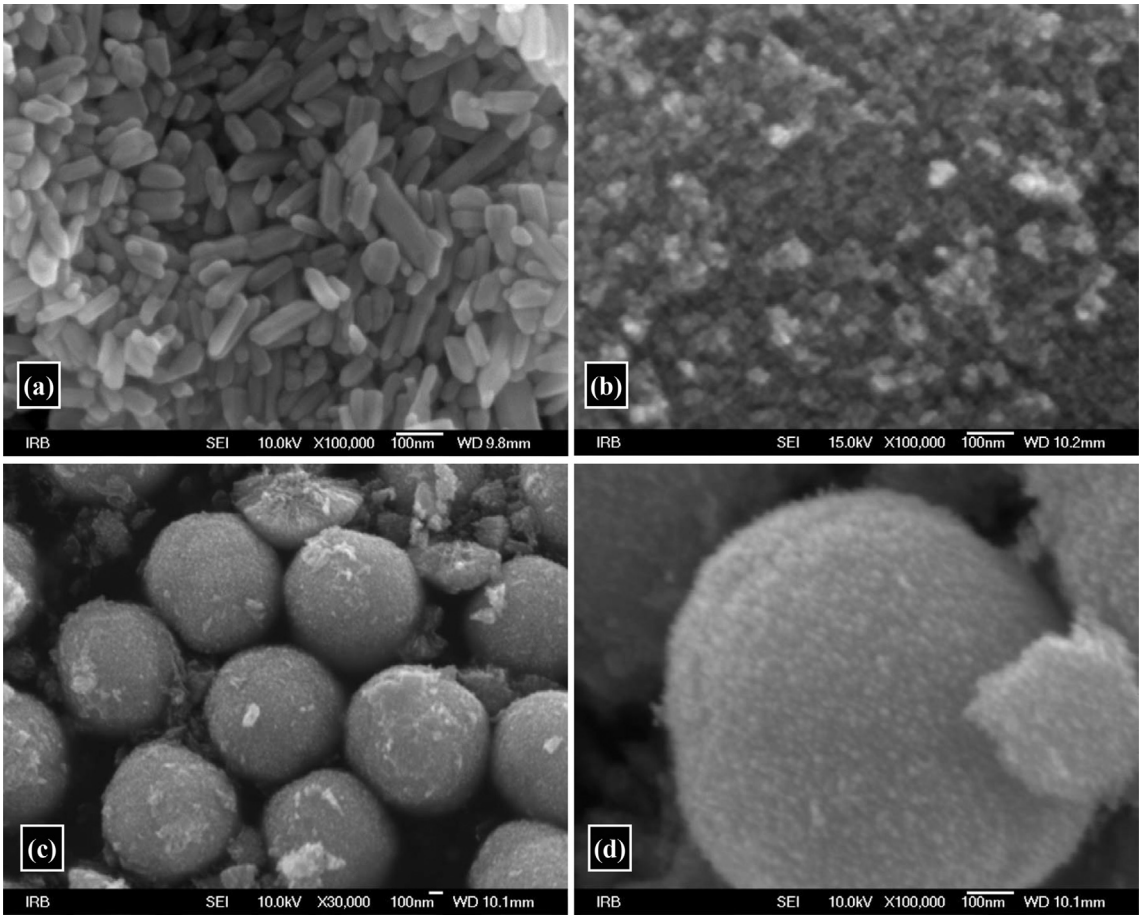


**Fig. 1.** FE-SEM images of samples: (a) E3, (b) ET3, (c, d) ET6 at different magnifications.

$[Zn(acac)_2] = 1{:}1$ consists of very big compact spheres formed by the aggregation of several smaller spheres. Small nanoparticles on the surface of these spheres are quite visible.

Fig. 4 shows the TEM/STEM images of sample ET2. The left panel shows well-dispersed slightly anisotropic nanoparticles having the mean particle size distribution of 16 nm as shown in the inset. The right upper panel shows a high resolution image (BF-STEM) of several stacking nanoparticles. A large nanoparticle in the middle of the panel exhibits crystal planes over the whole area notwithstanding different contrasts, indicating that the nanoparticle is monocrystalline. The right lower panel shows atomic resolution image.

### 3.2. X-ray diffraction line-broadening analysis

The results of XRD line-broadening analysis indicate the presence of size anisotropy with bigger crystallites in the direction of the c-ax of the zincite lattice compared with the direction perpendicular to the c-ax (Table 2, Fig. 5).

The values of the volume-averaged domain size ($D_v$) and the upper-limits of microstrains ($e$) were estimated from the results of Williamson-Hall analysis [17] by using the equation:

$$\left(\frac{\beta\cos\theta}{\lambda}\right) = \frac{K}{D_v} \times \left(\frac{4e\sin\theta}{\lambda}\right) \quad (1)$$

where $\lambda$ is the wavelength, $\beta$ stands for the physical broadening of the diffraction line and $K$ is the constant close to 0.9. The results of individual profile fitting (program XFIT) indicated the presence of size anisotropy with significantly narrower diffraction lines along the direction <00*l*> (Fig. 5). For that reason we separately estimated $D_v$ and $e$ values in the direction parallel to the *c*-ax, estimated from the $\beta$ values of the diffraction lines 002 and 004. The $\beta$ values were obtained by the convolution-fitting approach (program SHADOW [18]) in which the instrumental profile (diffraction lines of well-crystalline zincite powder) is convoluted with a refinable Voigt function to fit the observed profile. The obtained results of Williamson-Hall analysis are summarized in Table 2.

### 3.3. UV–Vis spectroscopy analysis

In order to investigate the optical properties of synthesized samples, the UV–Vis study was carried out. Fig. 6 shows the UV–Vis spectra of selected samples, their corresponding particle morphologies (inset) and calculated band gap values. The band gap values of ZnO samples were calculated using the procedure described by Dharma and Pisal [19]. The calculated band gap values for all synthesized samples are given in Table SI (Supplementary info). Fig. 6 shows that ZnO samples have no optical absorption in the visible region, but there is good absorption almost in the whole UV region. The UV–Vis spectra of ZnO samples are characterized by broad and intensive absorption between 400 and 250 nm with two superimposed maxima. One can see from Fig. 6 that the shape, position and relative intensity of superimposed maxima depend on the microstructural properties of synthesized ZnO samples. The red shift of the absorption edge and reduced band gap energies due to absorption closer to visible regions are clearly visible with the increased sample microsphere size. Recently a relationship

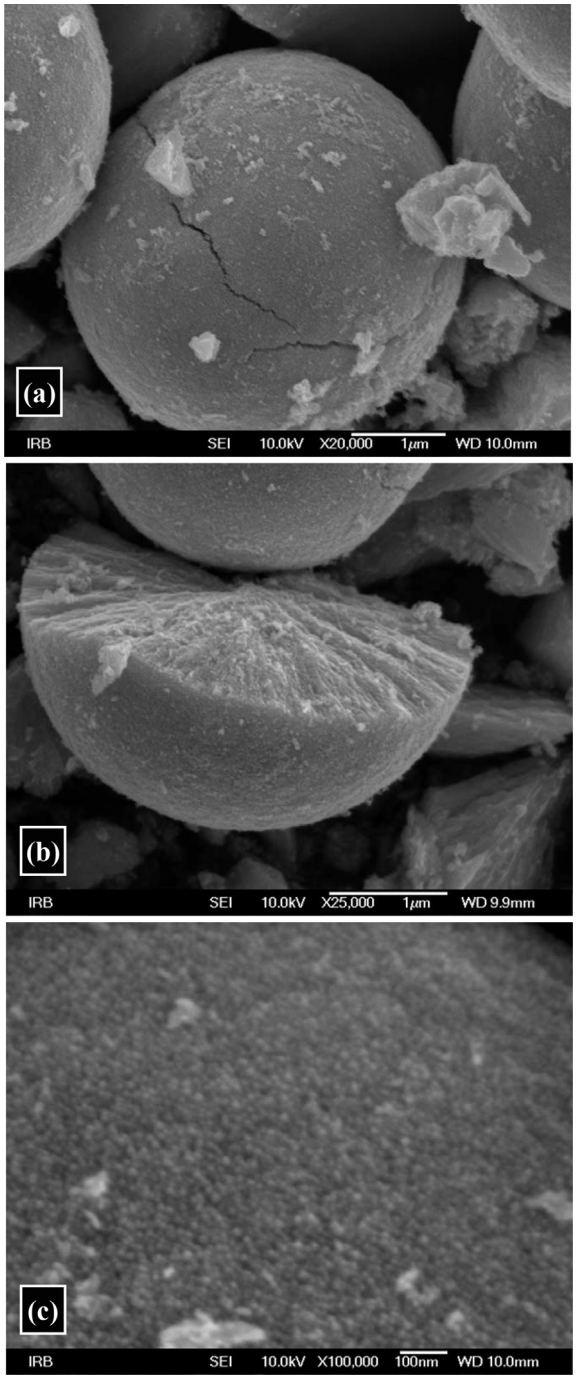


**Fig. 2.** FE-SEM images of sample ET8 in detail at different magnifications.

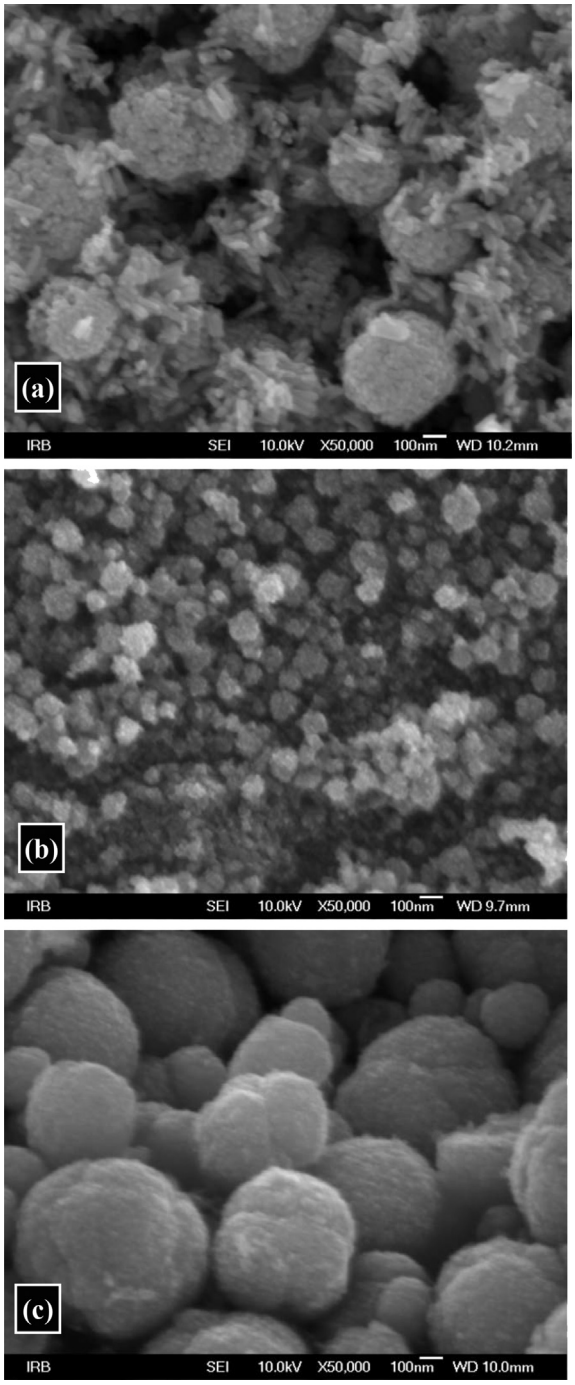


**Fig. 3.** FE-SEM images of samples: (a) O3, (b) OT3, (c) OT6.

between the particle size and optical properties of ZnO nanoparticles was investigated [20]. A significant increase in the absorption at a wavelength shorter than 400 nm can be assigned to the intrinsic bandgap adsorption of ZnO due to the electron transitions from the valence band to the conduction band [5]. The defects in the ZnO nanorods due to the "oriented attachment" of nanoparticles are the reason for a red-shifted absorption examined by the UV–Vis absorption spectrum [5].

### 3.4. FT-IR analysis

Fig. 7 shows the FT-IR spectra of selected ZnO samples. The left panel shows the FT-IR spectra of samples synthesized in the presence of ethanol, whereas the right panel shows the spectra of samples synthesized in the presence of octanol. The FT-IR bands between 540 and 390 $cm^{-1}$ with two poorly resolved bands are characteristic of ZnO. Furthermore, the FT-IR spectra of ZnO samples are characterized by the bands above 600 $cm^{-1}$ due to the adsorbed water and organic molecules. The IR band at ~1630 $cm^{-1}$ can be attributed to the bending vibration of $H_2O$ molecules adsorbed on ZnO particles. The FT-IR bands at 1582 to 1619 $cm^{-1}$, as well as the bands at 1385 to 1414 $cm^{-1}$, can be attributed to the asymmetrical and symmetrical stretching vibration of chemisorbed C=O bands originating from acetylacetonate [21]. The presented

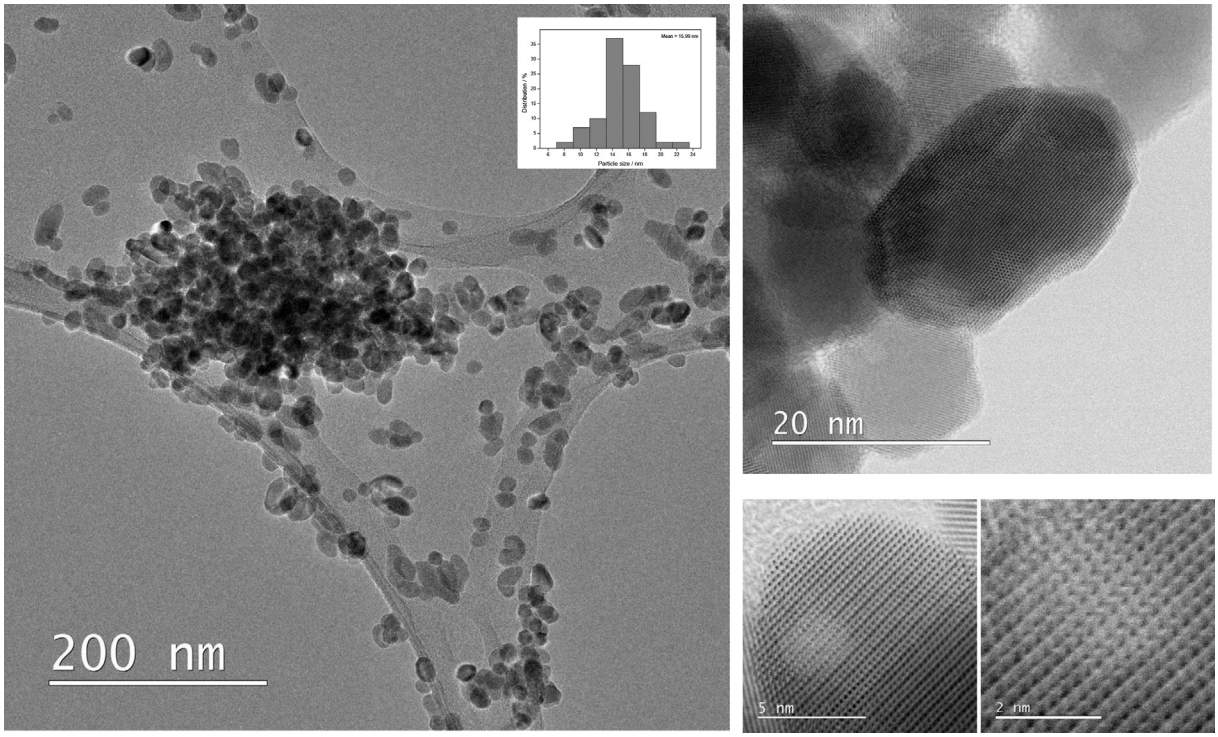


**Fig. 4.** TEM/BF-STEM images of sample ET2 in detail at different magnifications. Inset in the left panel shows particle size distribution.

FT-IR spectra indicate strong chemisorptions of carbonyl and carbonate groups on the surface of ZnO nanoparticles. Efafi et al. [20] used FTIR spectroscopy to investigate the surface of synthesized ZnO primarily sensitive to the surface reaction and found that ZnO also showed a C–N peak at 1000–1250 $cm^{-1}$ due to the reaction of TEA with zinc acetate. The presence of a C–H group from the precursor at 830 $cm^{-1}$ was also detectable.

## 4. Discussion

Generally, the formation of final ZnO particles could be divided into two stages: the nucleation continued with the growth of primary nanoparticles and immediately thereafter the microsphere aggregation. The presence of TEA had an effect on the nucleation as well as on the crystal growth of ZnO. TEA molecules combine the properties of amines which act as a weak base with a free electron pair on the nitrogen atom and alcohol with three hydroxyl branches. Therefore, TEA possesses a unique capability of undergoing reactions common to both groups.

It is assumed that the growth control of primary ZnO nanoparticles is established by the prevention of growth of nuclei in the first stage and continued by the prevention of growth of ZnO nanoparticles, which was achieved by a good adsorption of TEA on the particles. The addition of a small amount of TEA caused a radical change in the size of ZnO particles (Fig. 1a, b). Obviously, the surfaces of primary ZnO nanoparticles were covered with TEA molecules which slow down the particle growth. On doubling the molar ratio of TEA to $Zn(acac)_2$ in ethanol the precipitation of ZnO was delayed for more than 4 h, indicating the role of TEA chains in preventing the aggregation of ZnO seeds into primary nanoparticles. Owing to their long chains TEA and octanol together can provide a steric barrier between the ZnO particles, which allows stable dispersibility of the suspension without precipitation. Therefore, at the mole ratio $[TEA]/[Zn(acac)_2] = 1:1$ in octanol the precipitation of ZnO particles was delayed (it occurred after 24 h of ageing), whereas on doubling the molar ratio of TEA to $Zn(acac)_2$ the precipitation of ZnO was completely absent during 72 h of ageing. Clearly, octanol as a nonpolar long chain alcohol can slow down nucleation and prevent nanoparticle growth if taken together with a large amount of TEA.

In the second stage primary ZnO nanoparticles aggregated in assembled spheres whose size and shape depend on TEA concentration, ageing time and also the type of alcohol used. The growth mechanism of the obtained ZnO spheres is of complex nature. Spherical aggregation of ZnO particles is driven by means of noncovalent interactions such as hydrogen bonding, van der Waals

**Table 2**
Estimated values of the volume averaged domain sizes ($D_v$) and upper limits of microstrains ($e$) and the corresponding values in the directions parallel to the $c$-ax of zincite lattice as determined from the results of diffraction line broadening (Williamson-Hall analysis).

| Sample | $D_v$/nm | $e \times 10^3$ | $D_v \| c$-ax/nm | $e \times 10^3 \| c$-ax | Aspect ratio |
|---|---|---|---|---|---|
| E1 | 17(2) | 0.2(2) | 31(3) | 0.8(2) | 1.8 |
| E2 | 13(1) | 1.0(2) | 27(3) | 0.9(2) | 2.1 |
| E3 | 31(3) | 0.8(2) | >50 | 2.0(5) | >1.6 |
| ET1 | 9(1) | 0.6(2) | 19(2) | <0.2 | 2.1 |
| ET2 | 12(1) | 0.6(2) | 21(2) | <0.2 | 1.8 |
| ET3 | 16(1) | 0.2(2) | 22(2) | 0.6(2) | 1.4 |
| ET4 | 7(1) | <0.2 | 12(2) | 1.5(2) | 1.7 |
| ET5 | 9(1) | 0.3(2) | 21(2) | 1.6(2) | 2.3 |
| ET6 | 11(1) | 0.4(2) | 25(2) | 1.0(2) | 2.2 |
| ET8 | 11(1) | 0.7(2) | 24(2) | 0.5(2) | 2.2 |
| ET9 | 15(1) | 0.8(2) | 30(2) | 0.8(2) | 2 |
| O1 | 15(1) | 0.6(2) | 24(2) | <0.2 | 1.6 |
| O2 | 19(2) | 1.5(2) | 40(5) | 0.9(2) | 2.1 |
| O3 | 24(1) | 0.8(2) | 40(5) | <0.2 | 1.6 |
| OT1 | 5(1) | 0.3(2) | 9(1) | <0.2 | 1.8 |
| OT2 | 7(1) | <0.2 | 14(1) | 1.1(2) | 2 |
| OT3 | 7(1) | <0.2 | 14(1) | 0.6(2) | 2 |
| OT5 | 7(1) | 1.0(2) | 16(1) | <0.2 | 2.3 |
| OT6 | 13(1) | 1.0(2) | 30(2) | 0.7(2) | 2.3 |

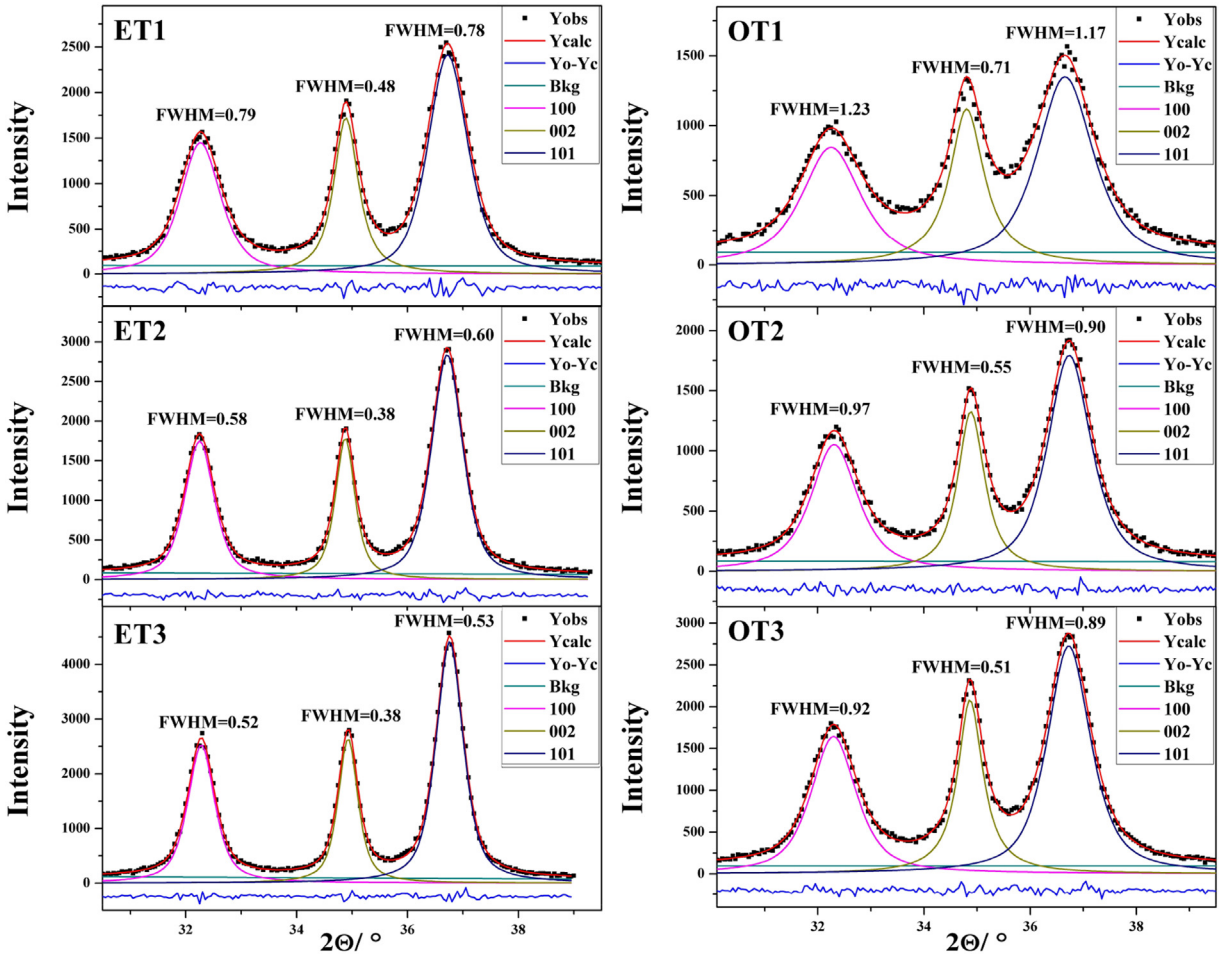


**Fig. 5.** Individual profile fitting results of samples ET1, ET2, ET3 (left panel) and samples OT1, OT2, OT3 (right panel).

forces and electrostatic forces. The formation of bigger densely packed ZnO spheres is favoured by increasing the TEA to $Zn(acac)_2$ mol ratio. The excess amount of TEA caused a too fast aggregation of primary ZnO nanoparticles. Doubling the molar ratio of TEA to $Zn(acac)_2$ in the presence of ethanol for 24 h favoured the formation of huge spherical aggregates (>3 μm) assembled from fine and uniform ZnO nanoparticles (~20 nm) (Fig. 2). The observed uniform dense packing of ZnO nanoparticles can also be attributed to the influence of small polar molecules of solvent (ethanol), while the cracking of huge spherical aggregates probably occurred due to the internal pressure associated with trapped solvent molecules and product gases (probably $CO_2$, NO, $H_2O$). Obviously the increase of TEA to $Zn(acac)_2$ mol ratio in the presence of ethanol favoured the aggregation of primary nanoparticles into bigger uniform regular spheres. Thus the excess amount of TEA had a different impact on the aggregation process. Ethanol as a small polar molecule, along with TEA molecules, is involved in the aggregation of primary ZnO nanoparticles. The most important driving forces responsible for the growth mechanism of ZnO spherical aggregates are diverse interactions of the solvent molecule as well as the TEA molecule with the surface of primary ZnO particles. These processes involve noncovalent interactions such as hydrogen bonding, the screening effect, etc. Due to the interaction between the TEA hydroxyl group and the surface of primary ZnO particles, the particle growth is limited on one side. On the other side, the remaining free hydroxyl groups of TEA molecules are attracted to each other by hydrogen bonding forces and serve as a link between neighbouring ZnO particles [11,13]. Thus the aggregation of ZnO nanoparticles into sphere in the second stage was achieved with a minimum of particle surface energy. Razali et al. [13] proposed the formation mechanism of microsphere ZnO nanostructures synthesized by the solvothermal method in diethanolamine (DEA). The formed ZnO nanoparticles were attracted to DEA chains due to an interaction between the hydrogen atoms in DEA and oxygen in ZnO. After that DEA chains were attracted to each other by hydrogen bonding forces and the seeds of a ZnO microsphere would be formed. Therefore, DEA acted as a bridge to form the ZnO microsphere and stopped the growth of ZnO nanoparticles. The morphology studies of samples prepared in monoethanolamine (MEA) and triethanolamine (TEA) confirm that DEA is a good polymer agent which plays an important role in preparing microsphere ZnO nanostructures. The effect of ethanolamine family on the morphology of ZnO nanoparticles is dependent on the number of hydroxyl branches. Xu et al. [11] discussed the formation mechanism of ZnO spheres formed by the agglomeration of nanoparticles synthesized by the hydrothermal method with different volume ratios of TEA to $H_2O$. The increases in the volume ratios of TEA to $H_2O$, used to control the diameter of ZnO spheres, favoured the formation of bigger densely packed ZnO spheres. The authors [11] emphasized that the presence of water in the hydrothermal system reduced the coordination ability of TEA molecule with $Zn^{2+}$. A similar formation mechanism has been reported [22] for the preparation of water-soluble $Fe_3O_4$

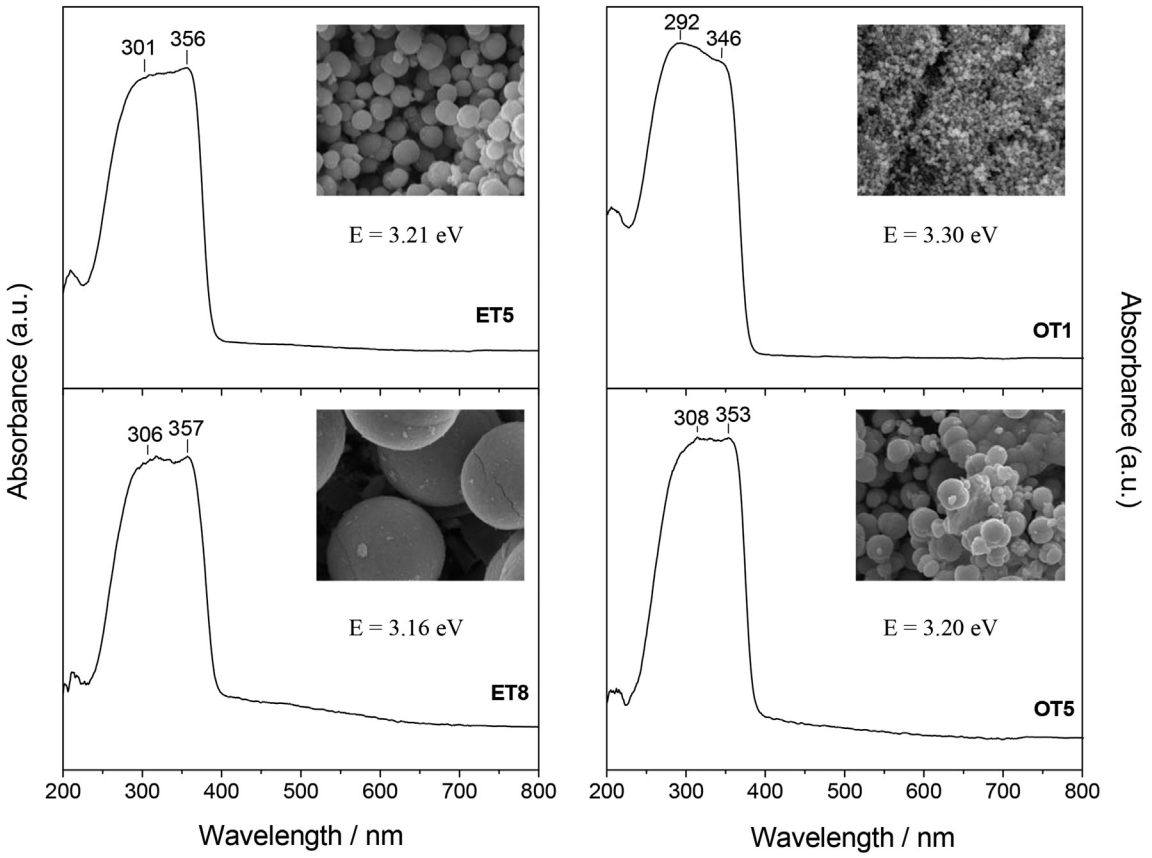


**Fig. 6.** UV–Vis spectra of samples ET5, ET8 (left panel) and samples OT1, OT5 (right panel). Inset images show the corresponding SEM images at the same magnification (10000×) and calculated band gap values.

sphere-like aggregate by the use of polyethylene glycol(5), nonylphenyl ether (NP5) and cyclodextrin (CD). Ambrožič et al. [23] proposed a formation mechanism of ZnO nanoparticles produced by starting from zinc acetylacetonate hydrate in organic media. They suggested that reaction proceeded via the alcoholytic C–C cleavage of the acetylacetonate ligand, which is promoted by water molecules present in the precursor and/or formed during polycondensation of the Zn–OH species. In this work, it is assumed that the intrinstically water from zinc acetylacetonate monohydrate is involved in ZnO nanoparticles formation.

Nonpolar molecules of octanol were involved in the aggregation of ZnO particles by weak van der Waals forces, whereas ethanol as a small polar molecule [24,25] could contribute to aggregation via reversible hydrogen bonding. For instance, weak van der Waals forces, as well as the steric barrier of long chain octanol, favoured the aggregation of primary nanosized iron oxide particles into irregular aggregates instead of regular spheres, as in the case of ethanol [24]. Park et al. [26] concluded that the polarity of the solvent is a key factor for the final particle size. A long-chain alcohol hinders hydrogen bonding and provides a repulsive force between particles. From the relationship between the dielectric constant and turbidity time the authors concluded that the reaction participating units are small oligomers rather than monomers.

Evidently, the addition of a small amount of TEA ([TEA]/[$Zn(acac)_2$] = 1:2) in the presence of octanol caused a significant reduction in particle size, not only of primary ZnO nanoparticles but also of their aggregates (Fig. 3b). The results of XRD analysis show that for the same experimental conditions the change of solvent from ethanol to octanol caused a reduction in the ZnO crystallite size (Fig. 5).

## 5. Conclusions

In this research we presented the impact of several important processing parameters (the presence of TEA as grown particle modifier and the presence of solvent molecules of different size and polarity) on the structural and microstructural properties of the obtained ZnO particles. The results of present investigation show a profound effect of surface interactions between the formed ZnO nanoparticles and the molecules of TEA and the solvent on the way of growth and aggregation, which enables the control of their morphological properties. TEA plays a crucial role in the control of the morphology and particle size of primary ZnO, acting both as a suppressor of primary ZnO nanoparticle growth which then aggregate into sphere, and also as a grown particle modifier of thus assembled nano/micron ZnO spheres. The formation of final ZnO particles could be divided into two stages; the growth of primary nanoparticles and immediately thereafter aggregation in microsphere.

It was established that the way of ZnO nanoparticle growth and their aggregation depend on the molar ratio [TEA]/[$Zn(acac)_2$] and the type of alcohol used as a solvent. The increase of the mole ratio of TEA to $Zn(acac)_2$ favoured the formation of bigger densely packed ZnO spheres. Doubling the molar ratio of TEA to $Zn(acac)_2$ in the presence of ethanol favoured the formation of huge spherical aggregates (>3 μm) assembled from fine and uniform ZnO nanoparticles (~20 nm).

The morphology and final particle size of obtained ZnO were dependent on the polarity of the solvent used. The presence of small polar molecules of ethanol in addition to TEA favoured the aggregation of big and densely packed ZnO spheres of regular shape. The results of XRD analysis show that for the same

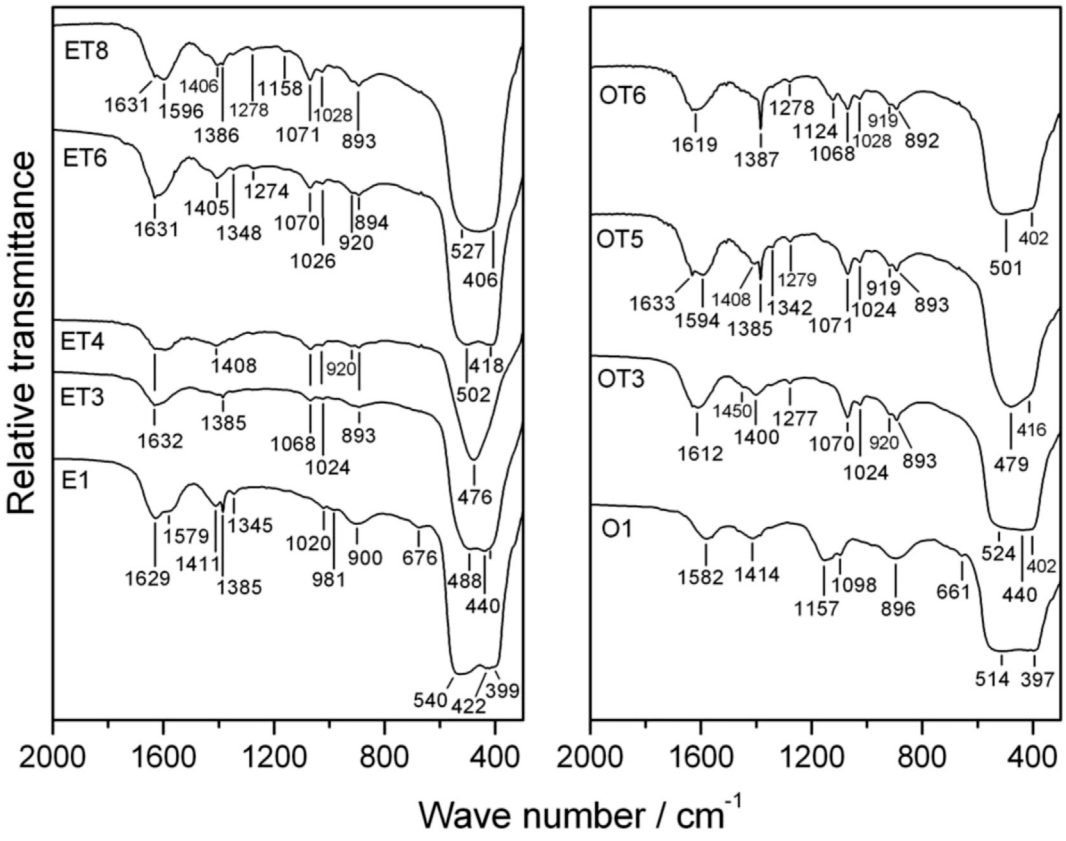


**Fig. 7.** Characteristic parts of the FT-IR spectra of samples E1, ET3, ET4, ET6, ET8 (left panel) and samples O1, OT3, OT5, OT6 (right panel).

experimental conditions the change of solvent from ethanol to octanol caused a reduction in the ZnO crystallite size. The results of size-strain analysis indicate the presence of size anisotropy.

Together, TEA and octanol can provide a steric barrier between ZnO particles, which allows a stable dispersibility of the suspension without precipitation. Therefore, at the mole ratio [TEA]/[$Zn(acac)_2$] = 1:1 the precipitation of ZnO particles was delayed (it occurred after 24 h of ageing), whereas at the mole ratio [TEA]/[$Zn(acac)_2$] = 2:1 the precipitation of ZnO was completely absent during 72 h of ageing.

## Appendix A. Supplementary data

Supplementary data related to this article can be found at http://dx.doi.org/10.1016/j.jallcom.2015.08.200.

## References

[1] M.R. Hoffmann, S.T. Martin, W. Choi, D.W. Bahnemann, Environmental applications of semiconductor photocatalysis, Chem. Rev. 95 (1995) 69–96, http://dx.doi.org/10.1021/cr00033a004.
[2] S. Sakthivel, B. Neppolian, M.V. Shankar, B. Arabindoo, M. Palanichamy, V. Murugesan, Solar photocatalytic degradation of azo dye: comparison of photocatalytic efficiency of ZnO and TiO2, Sol. Energy Mater. Sol. Cells 77 (2003) 65–82, http://dx.doi.org/10.1016/S0927-0248(02)00255-6.
[3] M. Vaseem, A. Umar, Y.-B. Hahn, ZnO nanoparticles: growth, properties, and applications, in: Metal Oxide Nanostructures and Their Applications, vol. 5, 2010, pp. 1–36.
[4] M. Andrès-Vergès, A. Mifsud, C.J. Serna, Formation of rod-like zinc oxide microcrystals in homogeneous solutions, J. Chem. Soc. Faraday Trans. 86 (1990) 959–963.
[5] L. Wu, Y. Wu, Synthesis and optical characteristic of ZnO nanorod, J. Mater. Sci. 42 (2007) 406–408, http://dx.doi.org/10.1007/s10853-006-0727-y.
[6] J. Yu, X. Yu, Hydrothermal synthesis and photocatalytic activity of zinc oxide hollow spheres, Environ. Sci. Technol. 42 (2008) 4902–4907, http://dx.doi.org/10.1021/es800036n.
[7] S. Cho, J.-W. Jang, S.-H. Jung, B.R. Lee, E. Oh, K.-H. Lee, Precursor effects of citric acid and citrates on ZnO crystal formation, Langmuir 25 (2009) 3825–3831.
[8] A. Šarić, S. Musić, M. Ivanda, Varying the microstructural properties of ZnO particles using different synthesis routes, J. Mol. Struct. 993 (2011) 219–224, http://dx.doi.org/10.1016/j.molstruc.2010.10.018.
[9] S. Musić, A. Šarić, S. Popović, Formation of nanosize ZnO particles by thermal decomposition of zinc acetylacetonate monohydrate, Ceram. Int. 36 (2010) 1117–1123, http://dx.doi.org/10.1016/j.ceramint.2009.12.008.
[10] S. Musić, A. Šarić, Formation of hollow ZnO particles by simple hydrolysis of zinc acetylacetonate, Ceram. Int. 38 (2012) 6047–6052, http://dx.doi.org/10.1016/j.ceramint.2012.04.020.
[11] S. Xu, Z.-H. Li, Q. Wang, L.-J. Cao, T.-M. He, G.-T. Zou, A novel one-step method to synthesize nano/micron-sized ZnO sphere, J. Alloys Comp. 465 (2008) 56–60, http://dx.doi.org/10.1016/j.jallcom.2007.10.095.
[12] A.K. Zak, R. Razali, W.H.A. Majid, M. Darroudi, Synthesis and characterization of a narrow size distribution of zinc oxide nanoparticles, Int. J. Nanomed. 6 (2011) 1399–1403, http://dx.doi.org/10.2147/IJN.S19693.
[13] R. Razali, A.K. Zak, W.H.A. Majid, M. Darroudi, Solvothermal synthesis of microsphere ZnO nanostructures in DEA media, Ceram. Int. 37 (2011) 3657–3663, http://dx.doi.org/10.1016/j.ceramint.2011.06.026.
[14] A.B. Kashyout, H.M.A. Soliman, H. Shokry Hassan, A.M. Abousehly, Fabrication of ZnO and ZnO: Sb nanoparticles for gas sensor applications, J. Nanomater. 2010 (2010) e341841, http://dx.doi.org/10.1155/2010/341841, 8 pp.
[15] Y.S. Fu, Y.F. Song, S.A. Kulinich, J. Sun, J. Liu, X.W. Du, Single-crystal ZnO flocky sphere formed by three-dimensional oriented attachment of nanoparticles, J. Phys. Chem. Solids 69 (2008) 880–883, http://dx.doi.org/10.1016/j.jpcs.2007.09.023.
[16] K.X. Yao, H.C. Zeng, ZnO/PVP nanocomposite spheres with two hemispheres, J. Phys. Chem. C 111 (2007) 13301–13308, http://dx.doi.org/10.1021/jp072550q.
[17] G.K. Williamson, W.H. Hall, Acta Metall. 1 (1953) 22–31.
[18] D.L. Bish, J.E. Post (Eds.), Modern Powder Diffraction, Reviews in Mineralogy, Mineralogical Society of America, Washington, 1989.
[19] J. Dharma, A. Pisal, Application Note, Simple Method of Measuring the Band Gap Energy Value of TiO2 in the Powder Form Using a UV/Vis/NIR Spectrometer, Perkin-Elmer Inc, Shelton, CT, USA, 2009.
[20] B. Efafi, M. Sasani Ghamsari, M.A. Aberoumand, M.H. Majles Ara, H. Hojati Rad, Highly concentrated ZnO sol with ultra-strong green emission, Mater. Lett. 111 (2013) 78–80, http://dx.doi.org/10.1016/j.matlet.2013.08.035.
[21] K. Nakamoto, Infrared and Raman Spectra of Inorganic and Coordination

Compounds, fourth ed., John Wiley & Sons, 1986.
[22] H.-B. Xia, J. Yi, P.-S. Foo, B. Liu, Facile fabrication of water-soluble magnetic nanoparticles and their spherical aggregates, Chem. Mater. 19 (2007) 4087–4091.
[23] G. Ambrožič, S.D. Škapin, M. Žigon, Z.C. Orel, The synthesis of zinc oxide nanoparticles from zinc acetylacetonate hydrate and 1-butanol or isobutanol, J. Coll. Interface Sci. 346 (2010) 317–323, http://dx.doi.org/10.1016/j.jcis.2010.03.001.
[24] M. Gotić, S. Musić, Synthesis of nanocrystalline iron oxide particles in the iron(III) acetate/alcohol/acetic acid system, Eur. J. Inorg. Chem. 2008 (2008) 966–973, http://dx.doi.org/10.1002/ejic.200700986.
[25] S. Sadasivan, A.K. Dubey, Y. Li, D.H. Rasmussen, Alcoholic solvent effect on silica synthesis—NMR and DLS investigation, J. Sol-Gel Sci. Tech. 12 (1998) 5–14, http://dx.doi.org/10.1023/A:1008659708390.
[26] J.S. Park, H.J. Hah, S.M. Koo, Y.S. Lee, Effect of alcohol chain length on particle growth in a mixed solvent system, J. Ceram. Process. Res. 7 (2006) 83.